ARTICLES

Journal of Semiconductors
(2023) 44, 032001
doi: 10.1088/1674-4926/44/3/032001

Bilayer MSe_2 (M = Zr, Hf, Mo, W) performance as a hopeful thermoelectric materials

Mahmood Radhi Jobayr[1, †] and Ebtisam M-T. Salman[2]

[1]Department of Radiology Technology, College of Health and Medical Technology, Middle Technical University (MTU), Baghdad, Iraq
[2]Department of Physics, College of Education for Pure Science (Ibn-AL-Haitham), University of Baghdad, Baghdad, Iraq

Abstract: Significant advancements in nanoscale material efficiency optimization have made it feasible to substantially adjust the thermoelectric transport characteristics of materials. Motivated by the prediction and enhanced understanding of the behavior of two-dimensional (2D) bilayers (BL) of zirconium diselenide ($ZrSe_2$), hafnium diselenide ($HfSe_2$), molybdenum diselenide ($MoSe_2$), and tungsten diselenide (WSe_2), we investigated the thermoelectric transport properties using information generated from experimental measurements to provide inputs to work with the functions of these materials and to determine the critical factor in the trade-off between thermoelectric materials. Based on the Boltzmann transport equation (BTE) and Bardeen-Shockley deformation potential (DP) theory, we carried out a series of investigative calculations related to the thermoelectric properties and characterization of these materials. The calculated dimensionless figure of merit (ZT) values of 2DBL-MSe_2 (M = Zr, Hf, Mo, W) at room temperature were 3.007, 3.611, 1.287, and 1.353, respectively, with convenient electronic densities. In addition, the power factor is not critical in the trade-off between thermoelectric materials but it can indicate a good thermoelectric performance. Thus, the overall thermal conductivity and power factor must be considered to determine the preference of thermoelectric materials.

Key words: ZT; thermoelectric property; 2D-bilayer; Boltzmann-transport equation; TE power factor

Citation: M R Jobayr and E M T Salman, Bilayer MSe_2 (M = Zr, Hf, Mo, W) performance as a hopeful thermoelectric materials[J]. *J. Semicond.*, 2023, 44(3), 032001. https://doi.org/10.1088/1674-4926/44/3/032001

1. Introduction

The increasing global demand for clean energy resources has led to interest in renewable energy resources as alternative energy sources that are cost-effective and environmentally acceptable. Thermoelectric materials have attracted researchers' interest because they satisfy the demand for sustainable energy, allowing direct conversion of thermal to electricity, as well as the potential for power generation and cooling[1–3]. Based on the Seebeck effect, the performance efficiency of thermoelectric materials is assessed by calculating their dimensionless figure of merit (ZT), which demonstrates their suitability as thermoelectric materials for practical applications[4, 5]. ZT is associated with the thermopower (Seebeck coefficient), S, electrical conductivity (σ), and total thermal conductivity of the material resulting from both electronic and lattice vibration (phononic) (κ_{ph}) contributions according to the following formula: $ZT = PF \cdot T/\kappa_{tot}$, where PF ($\equiv S^2\sigma$) is the power factor, and T is the operating temperature[6–11]. The electrical conductivity is related to the charge-carrier concentration (n), and the charge-carrier mobility (μ) is given by $\sigma = nq\mu$, where q is the carrier charge. Consequently, the factors affecting the superior performance of materials can be interlinked according to the following formula: $ZT = \left(S^2 n\right)\left(\mu/\kappa_e + \kappa_{ph}\right)qT$[1, 12].

The essential issue of developing and/or exploring innovative thermoelectric materials to achieve superior performance lies in two combinations of factors (S^2n), and (μ/κ_{tot}) on the same material[13]. Therefore, the main challenges are as follows: first, according to the Pisarenko relation, the more n, the lower the thermopower (or Seebeck coefficient, S); and second, although the charge-carrier mobility (μ) and total thermal conductivity (κ_{tot}) are interdependent, they are mutually opposite. Essentially, the maximum PF can be calculated from the two parameters, S and σ, which demonstrate inconsistent and opposing behaviors. Consequently, controlling both Seebeck coefficient and electrical conductivity simultaneously to enhance the power factor to find a meaningful improvement is a challenge. Novel strategies and paradigms to enhance the power factor and higher TE performance through optimal doping and band engineering[14, 15] or reducing κ_{ph} by nanostructural engineering[3, 16] have been proposed to improve the TE performance[17]. Based on these strategies, various high-efficiency two-dimensional (2D) thermoelectric materials have been reported, with nanostructures at various length scales. Meanwhile, 2D transition metal dichalcogenides (TMDCs) exhibit excellent performance and promising prospects for use in practical thermoelectric applications than their bulk counterparts[18–22]. Because the TMDCs have a layered system 2D crystal structures and these layers are interconnected and held together by weak van der Waals force, foreign atoms or molecules can be hosted into the gap (the so called van der Waals gap) forming various intercalated compounds. Intercalation is an effective and efficient means for electronic band structure manipulation[23, 24]. Among these materials, Bilayer MSe_2 (M = Mo, W, Hf, Zr) configurations have attracted attention because of their specific fea-

Correspondence to: M R Jobayr, dr.mahmood-radhi@mtu.edu.iq
Received 28 JULY 2022; Revised 17 SEPTEMBER 2022.

tures that give them an advantage over their peers. These materials possess degenerate conduction bands and an indirect bandgap with a high power factor[17]. The results of several studies related to the 2D configurations of TMDCs indicate variations in the thermoelectric performance[25–29]. For example, Wickramaratne *et al.*[30] did a theoretical study which investigates the electronic properties and the thermoelectric performance of bulk and one to four monolayers of four different transition-metal dichalcogenides (TMDCs) using density functional theory (DFT) with spin-orbit coupling and the Perdew-Burke-Ernzerhof (PBE). The results indicate among the four materials and four thicknesses, the $MoSe_2$ bilayer gives a maximum n-type ZT value of 2.4. In a study by Yan *et al.*[17] employing first-principles calculations combined with Boltzmann transport theory with van der Waals correction, the authors demonstrated that conduction band degeneracy and stair-like-shape density of state, which is absent in the bulk counterparts or monolayer, contribute to the high power factor.

In this study, we evaluated the TE properties of two-dimensional (2D) bilayer (BL) MSe_2 materials (M = Zr, Hf, Mo, or W). In addition, properties that enhance thermoelectric parameters are highlighted by utilizing the information generated in experimental measurements to provide input for working with the functionality of these materials. Therefore, precise and trustworthy calculations can be performed to aid in the prediction and understanding of the behavior of these materials, which is critical. Therefore, to solve the Boltzmann transport equation (BTE) and Bardeen–Shockley deformation potential (DP) theory, we will execute a series of investigative calculations related to the thermoelectric characteristics and characterization of these materials. The effects of some implicit parameters on the calculations of thermoelectric transport characteristics are discussed. In this regard, we can highlight the excellent advantages of bilayer thermoelectric materials and correlate them with their maximum figure of merit. These materials have been investigated for their superior electrical properties and low thermal conductivity. This helps to improve the experimental exploration of the thermoelectric properties of these materials.

2. Theoretical model

To evaluate the transport coefficients of the 2DBL-MSe_2 (M = Mo, W, Hf, Zr) structure, we integrated the relaxation times obtained from the single parabolic band (SPB) model with a semiclassical approach within the context of linearized Boltzmann transport theory[19, 29]. Consequently, the generalized Fermi integrals $\Pi^{(l)}$ are given by the following expressions[7, 29, 31]:

$$\Pi^{(l)} = \frac{N_V q^{2-l}}{2\pi}\int\left(-\frac{\partial f_k}{\partial E_k}\bigg|_{E=E_C}\right)\tau(k)\left(E(k)-E_F\right)^l v(k)\,v(k)\,\mathrm{d}k, \quad (1)$$

where f_k is equilibrium Fermi-Dirac distribution function, q is the electrical carrier charge, N_V is the valley degeneracy, $E(k)$ is the energy-wave vector dispersion relation, $v(k) \equiv (1/\hbar)\nabla_k E(k)$ represent the charge carriers velocity and $\hbar$ is the reduced Planck's constant. Meanwhile, f_k can be expressed in the following way[29, 31–33] :

$$f_k \equiv f_0(E) \equiv 1/[1+\exp(\eta_F)]\,. \quad (2)$$

In this equation, $\eta_F (= (E_F - E_C)/k_B T)$ is the dimensionless Fermi energy (reduced chemical potential), representing the position of the chemical potential (Fermi level) E_F relative to the lowest E_C conduction band, and k_B is the Boltzmann constant. Furthermore, the effective mass (m^*) near the Fermi energy is a critical parameter of thermoelectric transport, which has a significant impact on the values of the thermoelectric transport coefficients, and can be extracted from the following basic equation[34, 35]:

$$m^* = \hbar^2\left(\partial^2 E(k)/\partial^2 k\right)^{-1}. \quad (3)$$

Consequently, we find[25, 27, 29]

$$\Pi^{(l)} = \int_{E_o}^{\infty} -\frac{\partial f_0(E)}{\partial E}\eta_F^{(l)}\Xi(E)\,\mathrm{d}E, \quad (4)$$

where $\Xi(E)$ is transport distribution function, can be evaluated as[36]:

$$\Xi(E) = \sum_k \boldsymbol{v}_k \boldsymbol{v}_k \tau_k \delta(E - E_k)\,, \quad (5)$$

where $\boldsymbol{v}_k$ is the band-structure velocity, τ_k is the energy-dependent relaxation time, $\delta(E - E(k))$ is the delta function. Therefore, it can be deduced that this function connects the Seebeck coefficient and electrical conductivity. However, the measurable thermoelectric transport coefficients (σ, S, and κ_e) that emerge from a relaxation time approximation solution within the framework of the Boltzmann transport equation can be obtained by the following standard expressions[7, 37, 38] :

$$\sigma = q_o^2\,\Pi^{(0)} \quad \left(\Omega^{-1}\mathrm{m}^{-1}\right), \quad (6)$$

$$S = \frac{q_o k_B}{\sigma}\,\Pi^{(1)} \quad \left(\mathrm{VK}^{-1}\right). \quad (7)$$

The electronic thermal conductivity, κ_e, is defined as[11, 36]:

$$\kappa_e = \kappa_o - T\sigma S^2. \quad (8)$$

Here, $\kappa_o = k_B^2 T\,\Pi^{(2)}$, and therefore, κ_e can be written in terms of the integrals as

$$\kappa_e \equiv \frac{1}{q_o^2 T}\left\{\Pi^{(2)} - \Pi^{(1)}\left[\Pi^{(0)}\right]^{-1}\Pi^{(1)}\right\} \quad \left(\mathrm{Wm}^{-1}\mathrm{K}^{-1}\right). \quad (9)$$

According to the approach used in this study, the calculation of the energy-dependent relaxation time $\tau(E)$ has been done according to the Bardeen–Shockley deformation potential (DP) theory. However, this approach just takes into consideration acoustic phonon scattering although other scattering mechanisms such as impurities and polarization may be present[39–41]. The assumption of a unified relaxation time appears to be justified at room temperature, where electron scattering with acoustic phonons dominates in bilayer MSe_2 at moderate temperatures. This approach has been shown to be reliable in demonstrating the fine mobility of well-known 2DTE materials[17, 29, 42].

$$\tau(E) = \tau_0[E(k)/k_B T]^r, \quad (10)$$

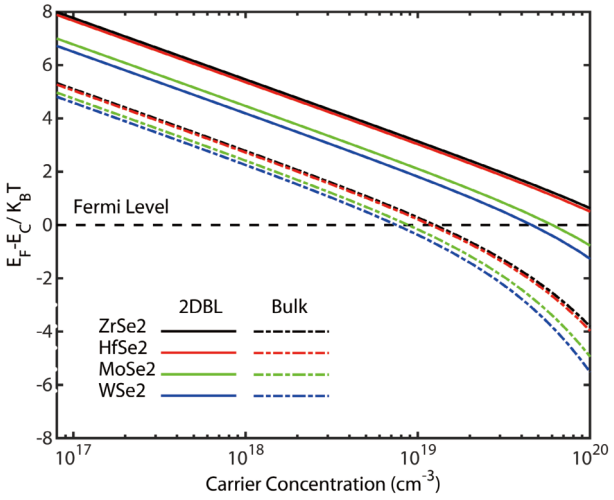

Fig. 1. (Color online) Reduced chemical potential versus carrier density for 2DBL MSe_2 (M = Zr, Hf, Mo, W) (solid line) and bulk (dotted line).

where r is the scattering parameter, which is determined according to the charge-scattering mechanism, $r = -1/2$ for subsequent calculations[17, 28, 34]. Accordingly, the relaxation time can be described by the following expression[29, 43]:

$$\langle \tau(E) \rangle = \frac{2^{1/2}\pi\hbar^4\rho v_l^2}{3E_d^2(m^* k_B T)^{3/2}} \frac{F_0(\eta_F)}{F_{1/2}(\eta_F)}, \tag{11}$$

where ρ is the mass density, E_d is the deformation potential, v_l is the longitudinal sound velocity, and F_i is the Fermi–Dirac integral of order i. In addition, F_i may play a more significant role in the study of semiconductors and can be expressed form[29, 32, 44]:

$$F_i(\eta_F) = \int_0^\infty \frac{\eta^i}{1+\exp(\eta-\eta_F)} d\eta. \tag{12}$$

If we assume that the electron relaxation time is direction-independent, which is a fairly good assumption even for anisotropic structures, the carrier mobility (μ) can be determined by $\mu = q\langle \tau(E) \rangle / m^*$[29]. The carrier concentration n is determined by[45, 46]:

$$n = \frac{(2m_d k_B T)^{3/2}}{2\pi^2\hbar^3} F_{1/2}(\eta_F), \tag{13}$$

where m_d denotes the average effective mass ($m_d = \sqrt{m_{\parallel} m_{\perp}}$). The following formula describes the relationship between Hall carrier mobility and electrical conductivity: $\mu_H = \sigma / q_0 n_H$, where n_H is inversely proportional to the Hall coefficient. In this model, τ is calculated by the deformation potential method as[30, 39, 40]

$$r_H = \frac{3}{4} \frac{F_{1/2}(\eta_F) F_{-1/2}(\eta_F)}{F_0(\eta_F)^2} F_{1/2}(\eta_F). \tag{14}$$

The acoustic phonon scattering mechanism governs the drift mobility, which is dependent on the chemical potential via[37, 39, 40] :

$$\mu = \frac{2^{1/2}\pi\hbar^4 e C_l N_V^{5/3}}{3m_d^{*5/2}(k_B T)^{3/2} D_f^2} \frac{F_0(\eta_F)}{F_{1/2}(\eta_F)}, \tag{15}$$

Table 1. The theoretical and experimental reported values of 2DBL-MSe_2 (M = Hf, Zr, Mo, W) that were used to evaluate the thermoelectric properties.

2DBL MX_2	$ZrSe_2$	$HfSe_2$	$MoSe_2$	WSe_2
m_x/m_o	2.88[17]	2.81[17]	0.539[30]	0.411[30]
m_y/m_o	0.66[17]	0.55[17]	0.539[30]	0.412[30]
C_{2D} (GPa)	318[42]	337[42]	494[42]	566[42]
D_f (eV)	1.25[42]	1.08[42]	3.65[42]	3.78[42]
(m_x/m_o), (m_y/m_o) (Bulk)	0.48[47]	0.42[47]	0.521[30]	0.489[30]
(m_z/m_o) (Bulk)	1.86[47]	2.17[47]	0.776[30]	0.643[30]
k_{ph} 2DBL (W/(m·K))	0.54[5]	0.51[5]	0.72[5]	0.66[5]
k_{ph} (Bulk) (W/(m·K))	9.9[17]	7.7[17]	52[30]	52[30]

where C_l is the elastic constant, D_f is the deformation potential coefficient, and N_V is the fold degeneration, which is almost four-fold.

3. Results and discussion

2DBL materials have potential benefits owing to their fascinating characteristics, which result from their distinctive traits and will be examined in further depth. We will now explore the power factor, Seebeck coefficient, electrical conductivity, thermal conductivity, and figure of merit in relationship to the TE characteristics. Electron concentrations are strongly related to the Fermi level, where the carrier density in the conduction and valence bands influences the Fermi level position, as shown in Fig. 1. Table 1 summarizes the theoretical and experimental values that were used in the calculations previously reported in several references for 2DBL-MSe_2 (M = Zr, Hf, Mo, W) and their bulk counterparts. First, we plotted the location of the Fermi level for the bulk (dashed dotted lines) and 2DBL-MSe_2 structures (solid lines) relative to the conduction band location vs. carrier concentration. It is obvious that η_F is larger (more negative) in 2D (solid lines) for all structures compared with their bulk counterparts (dashed dotted line). The Fermi level is located near the edges of the conduction bands and at close distances from each other in all bulk structures and at all concentrations. Very little variance was observed, particularly in the case of S, whereas 2D structures were located at different distances. Furthermore, at $n = 1 \times 10^{19}$ cm^{-3} carrier concentration, the Fermi level is extremely close to the band edges for all bulk structures but far away from the band edges for the 2DBL-MSe_2 structures.

At a carrier density of 1×10^{19} cm^{-3}, the E_F of both the $ZrSe_2$ (black line) and $HfSe_2$ (red line) bilayers was approximately $3k_BT$ higher than that of their bulk counterparts, whereas the E_F for both the $MoSe_2$ and WSe_2 bilayers was approximately $2k_BT$ higher than that of their bulk counterparts. This may appear to be paradoxical because a smaller number of sub-bands in the narrower 2D structure would have anticipated E_C to be closer to E_F at the same carrier density. Thus, the carrier density was standardized according to the thickness. When considering 2D at a certain carrier density and a specific η_F, if the number of sub-bands in the energy region of significance decreases linearly with the thickness of 2D, then η_F remains constant. When only one sub-band remains, decreasing the thickness does not affect the number of sub-bands. As the thickness decreased, η_F increased to maintain steady carrier density.

Moving on to the power factor of 2DBL-MSe_2 (M = Zr, Hf,

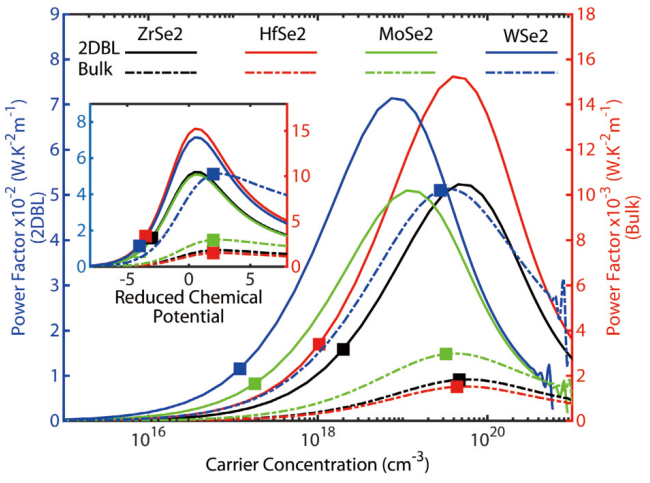

Fig. 2. (Color online) Thermoelectric power factor, PF, versus carrier density for 2DBL MSe_2 (M = Zr, Hf, Mo, W) (solid line) and bulk (dashed dot line). The square points represent the optimal values for obtaining ZT_{max} (the inset PF as a function of the reduced chemical potential).

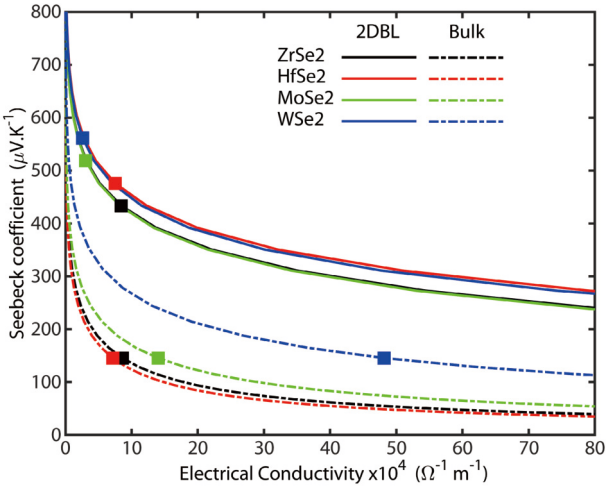

Fig. 3. (Color online) Seebeck coefficient versus electrical conductivity at T = 300 K for 2DBL MSe_2 (M = Zr, Hf, Mo, W) (solid line) and their bulk counterparts.

Mo, W), under the assumption of relaxation time according to the Bardeen-Shockley deformation potential (DP) theory, the power factor exhibits analogous behavior depending on the electron density (as shown in Fig. 2). The PF calculated for 2DBL-MSe_2 (M = Zr, Hf, Mo, W) showed peaks at carrier densities of $n = 5 \times 10^{19}$, 4×10^{19}, 1.5×10^{19}, and 8×10^{18} cm^{-3}, respectively. Generally, it is obvious that the value of PF for all 2DBL first increases to a maximum as a function of the carrier density, approximately $n \approx 1 \times 10^{19}$ cm^{-3} for $MoSe_2$ and WSe_2, whereas $n \approx 4 \times 10^{19}$ cm^{-3} for $ZrSe_2$ and $HfSe_2$, and then decreases with increasing n.

Furthermore, compared with their bulk counterparts, the power factor of each of the 2DBL structures was the most significant, which is a result of the high band degeneracy and low band effective mass[15]. By evaluating the PF values, it can be observed that the variation in these values is mostly related to conductivity, which includes many parameters that vary with various materials. Essentially, the variation in the behavior of different material bilayers in terms of S and σ stems from the location of the Fermi level with respect to their band edge (E_F) (see Fig. 1), which depends on the effective masses of the materials. The Seebeck coefficient versus electrical conductivity of 2DBL-MSe_2 (M = Zr, Hf, Mo, W) and its bulk counterparts are shown in Fig. 3. The electrical conductivity and Seebeck coefficient are inextricably linked by a clear inverserelationship.However,theelectronicstructureof2DBL-MSe_2 exhibits a stair-like density of state that is fundamentally different from that of its bulk counterparts, as well as being characterized by conduction band degeneracy[48]. Therefore, doping can play an effective role in the convergence of valence or conduction bands and thus increase the valley degeneracy, which causes an increase in electrical conductivity while maintaining the Seebeck coefficient[49]. This is explained by the fact that the smaller value of several bands dominates the Seebeck coefficient. The Seebeck coefficient is stable, but the electrical conductivity significantly rises if the degeneracy of many bands is attained[49, 50]. Consequently, band convergence is a practical method for enhancing a material's power factor[50]. In general, we clearly notice that the optimal values (square points) are within the carrier concentration range ($n \approx 10^{17}$–10^{20} cm^{-3}). The optimal values were located at the chemical potential values (–4, –3) (see inset of Fig. 2), which indicates that they were close to or inside the valence band. This depended on the type of material used at room temperature. We also noticed that the two materials $ZrSe_2$ and $HfSe_2$, with a heavy effective mass, had optimum values at concentrations of 5×10^{19} and 4×10^{19} cm^{-3}, respectively, corresponding to the position of the optimum chemical potential. While the optimum values for two materials, $MoSe_2$ and WSe_2, which have a heavy effective mass, are at concentrations of 1.5×10^{19} and 8×10^{18} cm^{-3}, respectively, corresponding to the position of the optimal chemical potential. As the conduction band edge (E_C) approaches the Fermi level, an improvement in the electrical conductivity is observed, while the Seebeck coefficient is negatively affected. As a result, the effect of electrical conductivity on the power factor is higher than that of the Seebeck coefficient. Two-dimensional 2D layers can benefit from the Seebeck coefficient, and thickness reduction has a greater effect on conductivity owing to improved scattering; therefore, the power factor is generally higher. At this concentration, the conduction band edge of $ZrSe_2$ is slightly outermost than the Fermi level, causing the power factor peak to appear at the 4.5×10^{19} cm^{-3} concentration, while the $HfSe_2$ peak appears asymptotic at a concentration of 4×10^{19} cm^{-3} concentration. This is due to various factors, including the influence of the electron effective mass on the Seebeck coefficient. For example, the larger effective mass of $ZrSe_2$, this, according to the Pisarenko relation, increases the Seebeck coefficient to a value higher than that of the other materials (see Fig. 3).

Many variables are important in defining the TE characteristics of bilayer materials. $HfSe_2$ exhibited significantly improved TE characteristics because of an increase in carrier density and electrical conductivity. Fig. 2 shows the location of the optimal values (square points) that lead to the maximum ZT values. We found that these points are relatively far from the peak power factor location; they are in the density range of 1×10^{17} and 1×10^{18} cm^{-3}. The square points in all figures indicate the optimal values for obtaining the maximum ZT value for 2DBL MSe_2 (M = Zr, Hf, Mo, W). However, if the max-

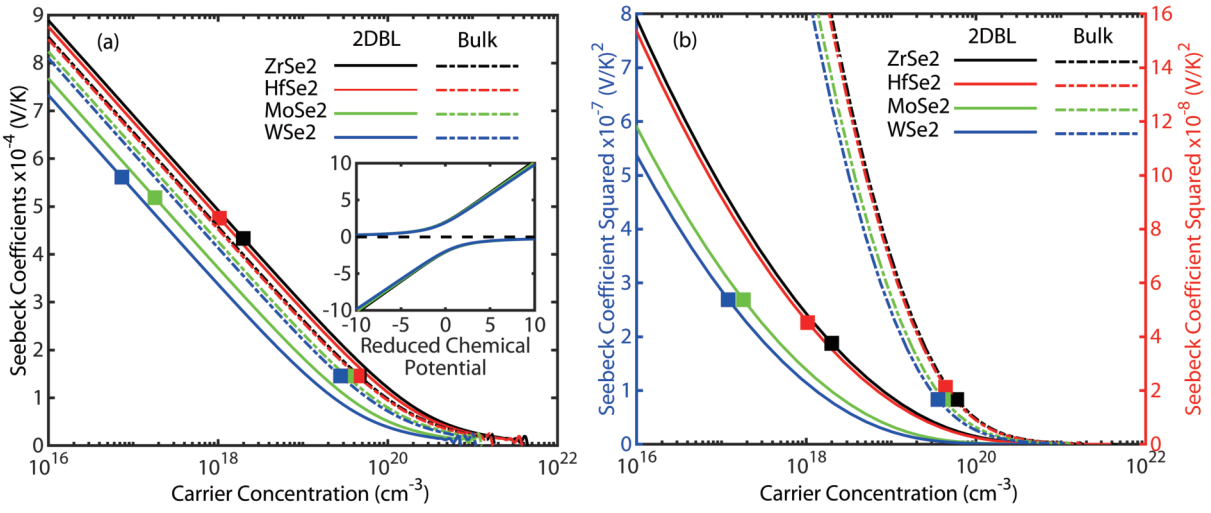

Fig. 4. (Color online) Carrier density dependence of absolute values of the Seebeck coefficient (Pisarenko relation) and the squared points represent the optimal values for obtaining (a) ZT_{max}, and (b) Seebeck coefficient squared for 2DBL MSe_2 (M = Zr, Hf, Mo, W) and bulk.

imum occurs at a high Fermi level, then it will equate to high concentration. A material with a high PF at unfeasible concentrations is useless.

In Fig. 4(a), according to the Pisarenko relationship, the Seebeck coefficient decreases monotonically with increasing carrier density of 2DBL-MSe_2 (M = Zr, Hf, Mo, W) and their bulk counterparts at T = 300 K. The Pisarenko relation serves as a guideline for assessing the effectiveness of improving the Seebeck coefficient for a particular carrier concentration and scattering mechanism. The higher value of the Seebeck coefficient observed in the $ZrSe_2$ material is immediately apparent, which is indicative of a large effective mass carrier density. This also applies to the squared S, as shown in Fig. 4(b). This was likely related to the reduced mobility associated with a large effective mass. For 2DBL-MSe_2 (M = Zr, Hf, Mo, W), the optimum values of the Seebeck coefficient leading to ZT_{max} are exhibited at 300 K in the range of 433–518 μV/K, corresponding to carrier concentrations of 7 × 10^{16}–2 × 10^{18} cm^{-3}. As shown in Fig. 4(a), the S differed slightly between these materials. This stems from the small difference in the effective electron masses of 2DBL-MSe_2 (M = Zr, Hf), which makes the S slightly different. In addition, for all materials, S converged with at n values greater than 10^{20}. This figure also shows that the optimal values of 2DBL-MSe_2 have Seebeck coefficients that correspond to the maximum values of the figure of merit. For $HfSe_2$ exhibit high ZT, the S at 300 K should be in the 475.87 μV/K, corresponding to carrier concentrations of 1 × 10^{18} cm^{-3}. The optimal S values for all materials and their bulk counterparts, which correspond to ZT_{max} at different concentrations, are listed in trations, are listed in Table 2. $HfSe_2$ possesses maximum and optimal power factors of 7.6179 and 1.7016 W/(K^2·m), respectively, which, combined with its low thermal conductivity, leads to high ZT values.

Mobility is an important physical quantity that can influence the calculations and preferences of materials, and is closely related to electrical conductivity. It is worth mentioning here that it is necessary to trade-off between the Seebeck coefficients on the one hand and the mobility on the other hand. As shown in Fig. 4, materials with the largest effective masses ($ZrSe_2$ and $HfSe_2$) had a positive effect on the Seebeck coefficient. Thus, it has a negative effect on electrical conductivity. According to the aforementioned relationship ($\mu = q\langle\tau(E)\rangle/m^*$), heavy carriers have lower mobility than light carriers, as shown in Fig. 5.

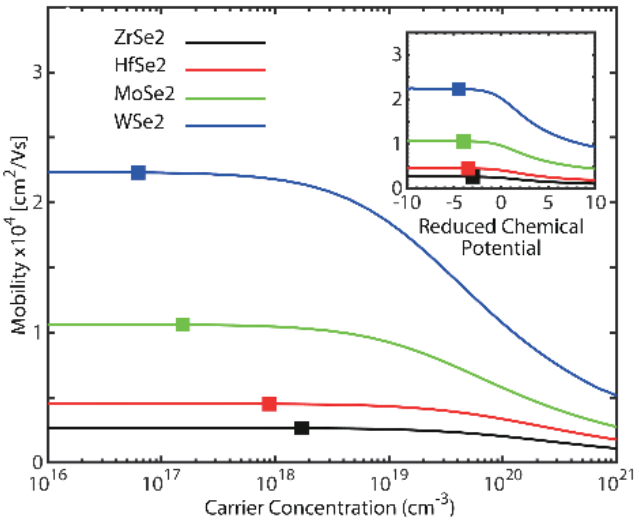

Fig. 5. (Color online) Mobility versus carrier density for 2DBL MSe_2 (M = Zr, Hf, Mo, W). The squared points represent the optimal values for obtaining ZT_{max} (the inset mobility as a function of the reduced chemical potential).

Therefore, there is a trade-off between the two. Furthermore, variations in the effective mass of these materials result in anisotropic transport. This is evident from the calculations of the average effective masses (m_d) for 2DBL $MoSe_2$, WSe_2, $HfSe_2$, and $ZrSe_2$ of 12.56m_o, 11.33m_o, 4.91m_o, and 3.75m_o, respectively. Theoretical calculations also showed that the mobility has a vital influence on the thermoelectric characteristics of 2DBL-MSe_2 (Zr, Hf, Mo, and W). According to Eq. (15), carrier mobility can be affected by more than the effective mass. Other implicit variables can also influence mobility, such as the deformation potential (DP) and elastic modulus (C_{2D}). Fig. 4 illustrates the carrier concentration dependence of the mobility for these structures (2DBL-MSe_2 and bulk), which is driven by the acoustic phonon scattering process. Based on the impact of these parameters, it is clear that

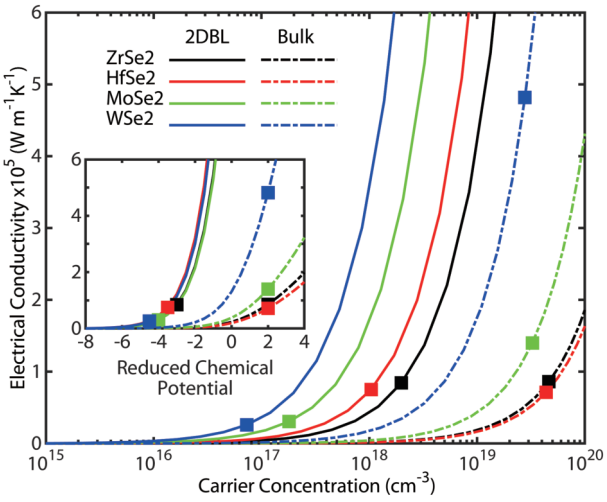

Fig. 6. (Color online) Electrical conductivity versus carrier density for 2DBL MSe_2 (M = Zr, Hf, Mo, W) (solid line) and bulk (dotted line. The squared points represent the optimal values for obtaining ZT_{max} (the inset σ as a function of the reduced chemical potential).

the mobility of 2DBL-WSe_2 is higher at higher concentrations. However, PF was not the highest among all materials tested. Fig. 5 shows the optimal mobility values (square points) at which the figure of merit peaks. It is important to note that although the mobility of materials such as 2DBL-$ZrSe_2$ and -$HfSe_2$ is lower than that of 2DBL-$MoSe_2$ and -WSe_2, their ZT values are substantially greater (as will be shown later). This implies that in addition to mobility, other variables play an important role in determining ZT values. ZT based on mobility is sometimes overestimated because acoustic phonons are not the sole component influencing mobility, which determines the final ZT.

By checking these assessments, one can see that the difference in electrical conductivity and consequently the maximum PF values for all materials are mostly related to mobility. A higher mobility always has a larger influence, resulting in high PF values compared to the effect of low mobility. This is directly related to the density of states being lower towards the top of the valence band than near the bottom of the conduction band. Furthermore, compared with their bulk counterparts, all 2DBL samples had the highest PF. However, the power factor exhibited variations based on the 2DBL structure. Thus, for $HfSe_2$, the maximum PF was as high as 7.6179 W/(K^2·m).

Fig. 6 clearly shows the direct relationship between electrical conductivity and charge density. As the carrier density increased, the Fermi EF level moved towards the conduction band. This is evident in the inset of Fig. 6. Interestingly, the electrical conductivity of 2DBL-MSe_2 (M = Mo, W) is lower than that of its bulk counterparts, whereas the values of MSe_2 (M = Zr, Hf) and their bulk counterparts are similar. It also clearly shows that the optimal value of the electrical conductivity of bulk WSe_2 is much higher than that of its 2D counterpart as well as that of other materials. However, this is not conclusive in determining the maximum ZT value, but it can indicate a good TE performance. As shown in Fig. 6, the optimal values of electrical conductivity for 2DBL-MSe_2 (M = Zr, Hf) are slightly higher than those for 2DBL-MSe_2 (M = Mo, W) because of their high effective mass. This leads to lower carrier

Table 2. Calculated values to obtain the maximum values of power factor for the 2DBL MSe_2 (M = Zr, Hf, Mo, W).

Material	m_d/m_o	τ (10^{-13} s)	μ (cm^2/(V·s))	PF_{max} (10^{-2})
$ZrSe_2$	1.26	3.12	0.0397	5.2357
$HfSe_2$	1.13	8.20	0.1158	7.6179
$MoSe_2$	0.49	11.09	0.3614	5.0970
WSe_2	0.37	16.94	0.7230	7.1409

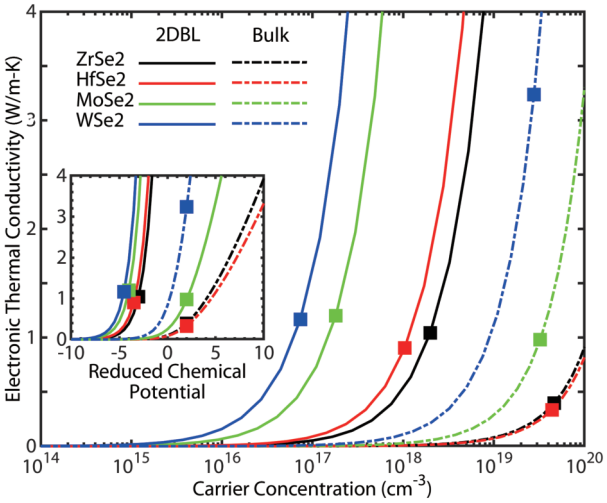

Fig. 7. (Color online) Electronic thermal conductivity versus carrier density for 2DBL MSe_2 (M = Zr, Hf, Mo, W) (solid line) and bulk (dotted line). The squared points represent the optimal values for obtaining ZT_{max} (the inset κ_e as a function of the reduced chemical potential).

mobility and, hence, lower electrical conductivity.

The monotonously increasing thermal conductivity, as shown in Fig. 7, led to the determination of the maximum ZT value of the studied materials. As mentioned previously, ZT is inversely correlated with κ_{tot}. To quantify the role of κ_{ph} in ZT, we used values from the available data, as shown in Table 2. However, the inverse correlation between ZT and κ_e was slightly stronger than that of κ_{ph} and ZT. These results illustrate the effect of κ_e on the TE performance of the 2DBL-MSe_2 structures. Because we assumed that κ_{ph} is constant, while κ_e calculated is large for all 2DBL-MSe_2 structures compared with κ_{ph}, κ_e is a critical parameter in determining the peak ZT. Overall, the contribution of κ_{ph} to the total thermal conductivity was only 34%–36%. Therefore, the total thermal conductivity significantly increased as a result of κ_e large contribution of κ_e. However, 2DBL-$HfSe_2$ has a smaller factor κ_{tot} (= κ_e+ κ_{ph}) than other 2DBL structures. Hence, the ZT value of $HfSe_2$ is superior to those of other materials.

To further verify the structural stability of these materials, Fig. 8 shows the phonon dispersion of 2DBL-MSe_2. One of the most useful aspects of phonon dispersion is the ability to check the structure's thermodynamic stability. The presence of phonon modes with positive (no imaginary) frequencies indicates that they appear to be thermodynamically stable, as seen in the phonon dispersion pattern throughout the entire Brillouin zone (see Fig. 8)[51, 52]. Additionally, it is evident from the estimated phonon dispersion that there is no soft mode, which confirms that the 2DBL MSe_2 (M = Zr, Hf, Mo, W) possess dynamic stability[17, 53]. Compared with the monolayer MSe_2 (M = Zr, Hf, Mo, W)[52, 53], the lattice phonon frequen-

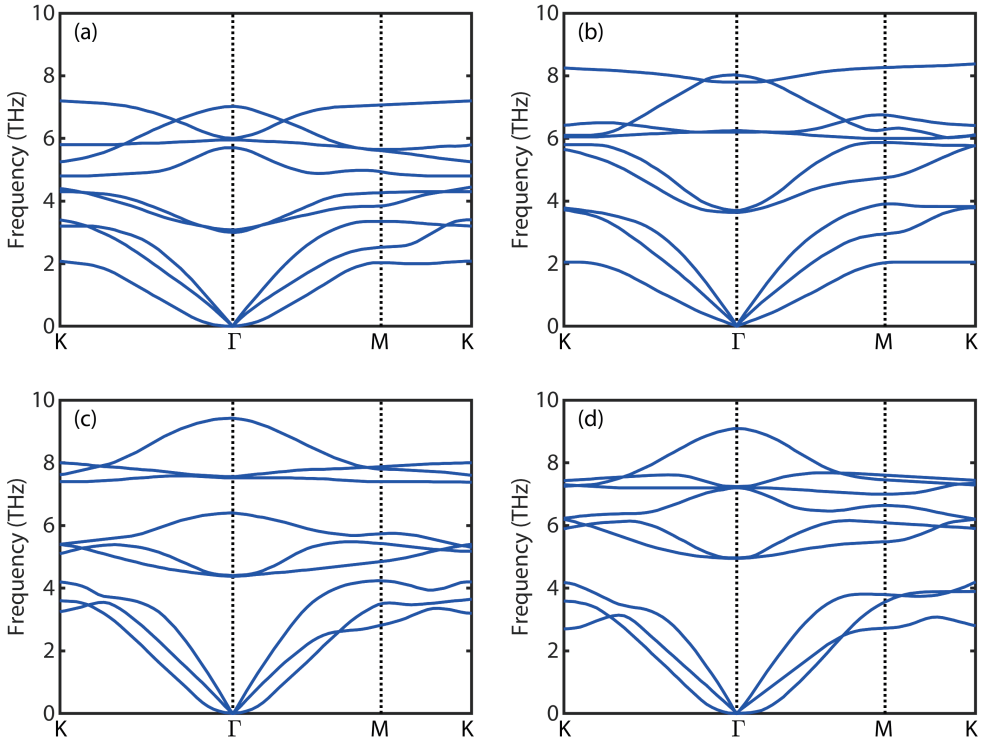

Fig. 8. (Color online) Phonon dispersions of bilayer. (a) $ZrSe_2$. (b) $HfSe_2$. (c) $MoSe_2$. (d) WSe_2.

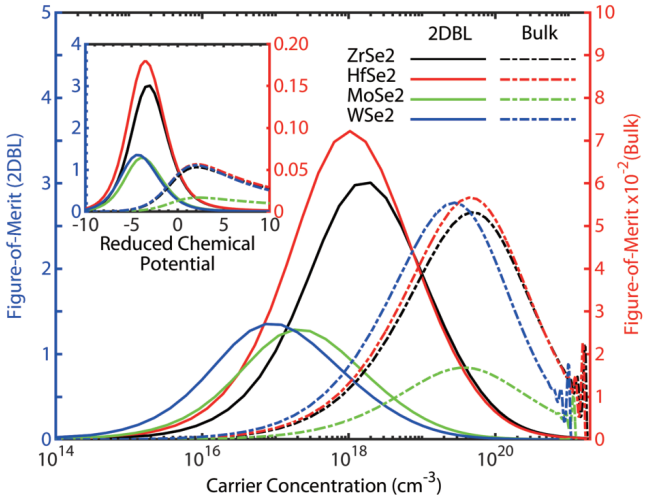

Fig. 9. (Color online) Figure of merit and carrier density of 2DBL-MSe_2 (M = Mo, W, Hf, Zr) (solid line) and bulk (dotted line) (inset ZT as a function of reduced chemical potential).

cies of the bilayer MSe_2 (M = Zr, Hf) exhibit smaller phonon frequencies, which can lead to low lattice thermal conductivity.

Finally, we explored the ZT values of 2DBL-MSe_2 (M = Zr, Hf, Mo, or W) and its bulk counterparts. Fig. 9 depicts these materials, with solid lines representing the 2DBL and dashed lines representing their bulk counterparts. From this figure, it can be seen that the ZT of the 2DBL-$ZrSe_2$ and $HfSe_2$ structures have maximum values of 3.01 and 3.61, respectively, which are much higher than the highest values of ZT for 2DBL-$MoSe_2$ and WSe_2 structures of 1.29 and 1.35, respectively. As shown in Table 3, these systems exhibit low κ_{tot}, which is advantageous for achieving the highest ZT value. It is generally observed that κ_{tot} results in an increasing ZT for 2DBL structures, reaching above 3.6 for $HfSe_2$.

This stems from the fact that κ_{tot} of $HfSe_2$ is too low to support an efficient ZT increase at 300 K. Although the values of ZT for $MoSe_2$ and WSe_2 exceed 1, possessing 1.29 and 1.35, respectively, which is a desirable condition, they are much lower than those of $HfSe_2$ and $ZrSe_2$. The lower ZT values of $MoSe_2$ and WSe_2 are mainly due to the fact that their high total thermal conductivity is larger than that of $HfSe_2$ and $ZrSe_2$. It is worth noting that $MoSe_2$ and WSe_2 achieved a remarkably high power factor, but their lattice thermal conductivities were higher than those of $ZrSe_2$ and $HfSe_2$; thus, their ZT values remained lower than those of $ZrSe_2$ and $HfSe_2$. According to the values in Table 2, a material with a higher power factor is not required to achieve a higher ZT value. We discovered that $MoSe_2$ and WSe_2 have higher power factors than $ZrSe_2$, but their figure of merit is lower.

4. Conclusions

In conclusion, we studied the thermoelectric performance of 2DBL-MSe_2 (M = Mo, W, Hf, Zr) by solving the Boltzmann transport equation (BTE) and Bardeen–Shockley deformation (DP) theory. Our focus was mainly on the thermoelectric parameters such as Seebeck coefficient, power factor, and thermal conductivity, which have been calculated at room temperature (300 K). Note that these materials have shown significant potential as high-quality thermoelectric materials at high temperatures due to their suitable band gap tunability, low dimensions, and the remarkable combination of electrical conductivity and lattice thermal conductivity[48, 53]. The results show that these materials possess impressive ZT values that are much higher than those of their bulk counterparts. In addition, the emergence of thermal conductivity is a critical factor in determining the ZT peak of these materials, with a relatively low values of 1.582, 1.414, 1.989, and 1.828 W/(m·K) for 2DBL MSe_2 (M = Mo, W, Hf, Zr). By combining the thermal conductivity with the power factor and making favorable improvements in the electronic properties, the

Table 3. Calculated properties of 2DBL-MSe_2 (M = Zr, Hf, Mo, W) and their bulk counterparts.

Material	$ZrSe_2$		$HfSe_2$		$MoSe_2$		WSe_2	
	2DBL	Bulk	2DBL	Bulk	2DBL	Bulk	2DBL	Bulk
n_{opt} (10^{17} cm^{-3})	20	464	10	438	2	325	0.7	278
μ_{opt} ($cm^2/(V{\cdot}s)$)	2652	116[54]	4519	102[54]	10609	269[54]	22304	1083[54]
S_{opt} ($\mu V/K$)	−433.54	−145.64	−475.87	−145.64	−518.5	−145.64	−561.3	−145.64
σ_{opt} (10^4 $\Omega^{-1}m^{-1}$)	8.435	8.6090	7.514	7.1545	3.067	13.9965	2.616	48.144
PF_{opt} (10^{-2} $W/(K^2{\cdot}m)$)	1.5854	0.18261	1.7016	1.5176	0.8246	0.2969	0.8242	1.0212
K_e ($W/(K{\cdot}m)$)	1.042	0.3968	0.904	0.3354	1.202	0.9798	1.168	3.2370
K_{tot} ($W/(K{\cdot}m)$)	1.582	10.2968	1.414	8.0354	1.922	52.9798	1.828	55.2370
ZT (dimensionless)	3.01	0.0532	3.61	0.0567	1.29	0.0168	1.35	0.0555

ZT reaches 3.6 and 3.0 for $HfSe_2$ and $ZrSe_2$, respectively. The $HfSe_2$ and $ZrSe_2$ bilayers, which have lower electronic thermal conductivity than the other two materials, have shown exceptional promise for thermoelectric performance compared to the $MoSe_2$ and WSe_2 bilayers, which have ZT of up to 1.29 and 1.35, respectively. Remarkably, WSe_2 had the second highest PF peak, but its ZT peak ranked third among the four materials evaluated. Furthermore, the difference ratio between the ZT peaks of these materials is not the same as that of the power factor. Therefore, we reported that the κ_{tot} and PF must be coupled to determine the order of preference for thermoelectric materials. In addition, we found that the effect of electrical conductivity on the PF was greater than that of the Seebeck coefficient. In addition, as the conduction band edge (E_C) approaches the Fermi level, an electrical conductivity improvement appears, while the Seebeck coefficient is negatively affected. Moreover, it is evident from the location of the optimal values (square points) for all parameters that lie within the range of acceptable achievable concentrations, which is proportional to the location of the Fermi level relative to the E_C edge. As a result, all of the materials' maximum ZT values were found to be within the acceptable concentration levels.

References

[1] Heremans J P. Introduction to cryogenic solid state cooling. Tri-Technology Device Refrigeration (TTDR), 2016, 9821, 95

[2] Finefrock S W, Yang H R, Fang H Y, et al. Thermoelectric properties of solution synthesized nanostructured materials. Annu Rev Chem Biomol Eng, 2015, 6, 247

[3] Wang X, Shi Y Q, Ding L M. To enhance the performance of n-type organic thermoelectric materials. J Semicond, 2022, 43, 020202

[4] He J, Tritt T M. Advances in thermoelectric materials research: Looking back and moving forward. Science, 2017, 357, eaak9997

[5] Özbal G, Senger T, Sevik C, et al. Ballistic thermoelectric properties of monolayer semiconducting transition metal dichalcogenides and oxides. Phys Rev B, 2019, 100, 084515

[6] Esfarjani K, Zebarjadi M, Kawazoe Y. Thermoelectric properties of a nanocontact made of two-capped single-wall carbon nanotubes calculated within the tight-binding approximation. Phys Rev B, 2006, 73, 085406

[7] Farhangfar S. Size-dependent thermoelectricity in nanowires. J Phys D, 2011, 44, 125403

[8] Hung N T, Nugraha A R T, Saito R. Two-dimensional InSe as a potential thermoelectric material. Appl Phys Lett, 2017, 111, 092107

[9] Zhu X L, Liu P F, Zhang J R, et al. Monolayer SnP_3: An excellent p-type thermoelectric material. Nanoscale, 2019, 11, 19923

[10] Skelton J M, Parker S C, Togo A, et al. Thermal physics of the lead chalcogenides PbS, PbSe, and PbTe from first principles. Phys Rev B, 2014, 89, 205203

[11] Gao Z B, Wang J S. Thermoelectric penta-silicene with a high room-temperature figure of merit. ACS Appl Mater Interfaces, 2020, 12, 14298

[12] Ceyda Yelgel Ö, Srivastava G P. Thermoelectric properties of p-type $(Bi_2Te_3)_x(Sb_2Te_3)_{1-x}$ single crystals doped with 3 wt.% Te. J Appl Phys, 2013, 113, 073709

[13] Heremans J P, Wiendlocha B, Chamoire A M. Resonant levels in bulk thermoelectric semiconductors. Energy Environ Sci, 2012, 5, 5510

[14] Zhu T J, Liu Y T, Fu C G, et al. Compromise and synergy in high-efficiency thermoelectric materials. Adv Mater, 2017, 29, 1605884

[15] Fang T, Zheng S Q, Zhou T, et al. Computational prediction of high thermoelectric performance in p-type half-Heusler compounds with low band effective mass. Phys Chem Chem Phys, 2017, 19, 4411

[16] Wang R Y, Feser J P, Lee J S, et al. Enhanced thermopower in PbSe nanocrystal quantum dot superlattices. Nano Lett, 2008, 8, 2283

[17] Yan P, Gao G Y, Ding G Q, et al. Bilayer MSe_2 (M = Zr, Hf) as promising two-dimensional thermoelectric materials: A first-principles study. RSC Adv, 2019, 9, 12394

[18] Li S, Wang Y M, Chen C, et al. Heavy doping by bromine to improve the thermoelectric properties of n-type polycrystalline SnSe. Adv Sci, 2018, 5, 1800598

[19] Kim S, Lee C, Lim Y S, et al. Investigation for thermoelectric properties of the MoS_2 monolayer-graphene heterostructure: Density functional theory calculations and electrical transport measurements. ACS Omega, 2020, 6, 278

[20] Kara H, Upadhyay Kahaly M, Özdoğan K. Thermoelectric response of quaternary Heusler compound CrVNbZn. J Alloys Compd, 2018, 735, 950

[21] Wu X M, Ke X X, Sui M L. Recent progress on advanced transmission electron microscopy characterization for halide perovskite semiconductors. J Semicond, 2022, 43, 041106

[22] Jobayr M R, Salman E M T. Investigation of the thermoelectric properties of one-layer transition metal dichalcogenides. Chin J Phys, 2021, 74, 270

[23] Wu D, Huang L, Jia P Z, et al. Tunable spin electronic and thermoelectric properties in twisted triangulene π-dimer junctions. Appl Phys Lett, 2021, 119, 063503

[24] Chen X K, Hu X Y, Jia P, et al. Tunable anisotropic thermal transport in porous carbon foams: The role of phonon coupling. Int J Mech Sci, 2021, 206, 106576

[25] Zhao Q Y, Guo Y H, Si K Y, et al. Elastic, electronic, and dielectric properties of bulk and monolayer ZrS_2, $ZrSe_2$, HfS_2, $HfSe_2$ from van der Waals density-functional theory. Phys Status Solidi B, 2017, 254, 1700033

[26] Qin D, Ge X J, Ding G Q, et al. Strain-induced thermoelectric performance enhancement of monolayer $ZrSe_2$. RSC Adv, 2017, 7, 47243

[27] Yao Q R, Zhang L J, Bampoulis P, et al. Nanoscale investigation of defects and oxidation of $HfSe_2$. J Phys Chem C, 2018, 122, 25498
[28] Ju L, Bie M, Shang J, et al. Janus transition metal dichalcogenides: A superior platform for photocatalytic water splitting. J Phys Mater, 2020, 3, 022004
[29] Guo R Q, Wang X J, Kuang Y D, et al. First-principles study of anisotropic thermoelectric transport properties of IV-VI semiconductor compounds SnSe and SnS. Phys Rev B, 2015, 92, 115202
[30] Wickramaratne D, Zahid F, Lake R K. Electronic and thermoelectric properties of few-layer transition metal dichalcogenides. J Chem Phys, 2014, 140, 124710
[31] Witkoske E, Wang X, Maassen J, et al. Universal behavior of the thermoelectric figure of merit, zT, *vs.* quality factor. Mater Today Phys, 2019, 8, 43
[32] Koroleva O N, Mazhukin A V, Mazhukin V I, et al. Approximation of Fermi-Dirac integrals of different orders used to determine the thermal properties of metals and semiconductors. Mathematica Montisnigri, 2016, 35, 37
[33] Hernandez J A, Ruiz A, Fonseca L F, et al. Thermoelectric properties of SnSe nanowires with different diameters. Sci Rep, 2018, 8, 11966
[34] Qin D, Yan P, Ding G Q, et al. Monolayer $PdSe_2$: A promising two-dimensional thermoelectric material. Sci Rep, 2018, 8, 2764
[35] Wang X F, Askarpour V, Maassen J, et al. On the calculation of Lorenz numbers for complex thermoelectric materials. J Appl Phys, 2018, 123, 055104
[36] Scheidemantel T J, Ambrosch-Draxl C, Thonhauser T, et al. Transport coefficients from first-principles calculations. Phys Rev B, 2003, 68, 125210
[37] Neophytou N, Kosina H. Effects of confinement and orientation on the thermoelectric power factor of silicon nanowires. Phys Rev B, 2011, 83, 245305
[38] Chen J M, Wang D, Shuai Z G. First-principles predictions of thermoelectric figure of merit for organic materials: Deformation potential approximation. J Chem Theory Comput, 2012, 8, 3338
[39] Wu C W, Ren X, Xie G F, et al. Enhanced high-temperature thermoelectric performance by strain engineering in BiOCl. Phys Rev Appl, 2022, 18, 014053
[40] Jia P Z, Xie Z X, Deng Y X, et al. High thermoelectric performance induced by strong anharmonic effects in monolayer $(PbX)_2$ (X = S, Se, Te). Appl Phys Lett, 2022, 121, 043901
[41] Ganose A M, Park J, Faghaninia A, et al. Efficient calculation of carrier scattering rates from first principles. Nat Commun, 2021, 12, 2222
[42] Zhang W X, Huang Z S, Zhang W L, et al. Two-dimensional semiconductors with possible high room temperature mobility. Nano Res, 2014, 7, 1731
[43] Tang L, Long M Q, Wang D, et al. The role of acoustic phonon scattering in charge transport in organic semiconductors: A first-principles deformation-potential study. Sci China Ser B, 2009, 52, 1646
[44] Yadav A, Deshmukh P C, Roberts K, et al. An analytic study of the Wiedemann-Franz law and the thermoelectric figure of merit. J Phys Commun, 2019, 3, 105001
[45] Chen C L, Wang H, Chen Y Y, et al. Thermoelectric properties of p-type polycrystalline SnSe doped with Ag. J Mater Chem A, 2014, 2, 11171
[46] Jia T T, Feng Z Z, Guo S P, et al. Screening promising thermoelectric materials in binary chalcogenides through high-throughput computations. ACS Appl Mater Interfaces, 2020, 12, 11852
[47] Yumnam G, Pandey T, Singh A K. High temperature thermoelectric properties of Zr and Hf based transition metal dichalcogenides: A first principles study. J Chem Phys, 2015, 143, 234704
[48] Bittner M, Kanas N, Hinterding R, et al. A comprehensive study on improved power materials for high-temperature thermoelectric generators. J Power Sources, 2019, 410/411, 143
[49] Pei Y Z, Shi X Y, LaLonde A, et al. Convergence of electronic bands for high performance bulk thermoelectrics. Nature, 2011, 473, 66
[50] Wolf M, Hinterding R, Feldhoff A. High power factor *vs.* high zT—A review of thermoelectric materials for high-temperature application. Entropy, 2019, 21, 1058
[51] Liu X, Zhang D B, Wang H, et al. Ultralow lattice thermal conductivity and high thermoelectric performance of penta-Sb_2C monolayer: A first principles study. J Appl Phys, 2021, 130, 185104
[52] Zhen Y X, Yang M, Zhang H, et al. Ultrahigh power factors in P-type 1T-ZrX_2 (X = S, Se) single layers. Sci Bull, 2017, 62, 1530
[53] Huang Z S, Zhang W X, Zhang W L. Computational search for two-dimensional MX_2 semiconductors with possible high electron mobility at room temperature. Materials, 2016, 9, 716
[54] Qian X, Yang R G. Temperature effect on the phonon dispersion stability of zirconium by machine learning driven atomistic simulations. Phys Rev B, 2018, 98, 224108

Mahmood Radhi Jobayr is an Assistant Professor of Physics at the Middle Technical University in Baghdad. His research focuses on the physics of materials, semiconductors, and narrow-gap metals. He is interested in theoretical solid state physics, focusing on calculations of electronic structure, superconducting and thermoelectric properties.

Ebtisam M-T. Salman is an Assistant Professor of Physics at the University of Baghdad. She is currently a researcher and lecturer in the physics department. Her research focuses on the physics of semiconductors and lasers, particularly on semiconductor laser, optical, thermal, electronic, and thermoelectric transport properties.